Widespread air pollutants of the North China Plain during the Asian summer monsoon season: A case study

Jiarui Wu[1,3], Naifang Bei[2], Xia Li[1,3], Junji Cao[1*], Tian Feng[1], Yichen Wang[1], Xuexi Tie[1], and Guohui Li[1*]

[1]Key Lab of Aerosol Chemistry and Physics, SKLLQG, Institute of Earth Environment, Chinese Academy of Sciences, Xi'an, China
[2]School of Human Settlements and Civil Engineering, Xi'an Jiaotong University, Xi'an, Shaanxi, China
[3]University of Chinese Academy of Science, Beijing, China

[*]Correspondence to: Guohui Li (ligh@ieecas.cn) and Junji Cao (jjcao@ieecas.cn)

Abstract: During the Asian summer monsoon season, prevailing southeasterly - southwesterly winds are subject to delivering air pollutants from the North China Plain (NCP) to the Northeast and Northwest China. In the present study, the WRF-CHEM model is used to evaluate contributions of trans-boundary transport of the NCP emissions to the air quality in the Northeast and Northwest China during a persistent air pollution episode from 22 to 28 May 2015. The WRF-CHEM model generally performs well in capturing the observed temporal variation and spatial distribution of fine particulate matters ($PM_{2.5}$), ozone (O_3), and NO_2. The simulated temporal variation of aerosol species is also in good agreement with measurements in Beijing during the episode. Model simulations show that the NCP emissions contribute substantially to the $PM_{2.5}$ level in Liaoning and Shanxi provinces, the adjacent downwind areas of the NCP, with an average of 24.2 and 13.9 μg m^{-3} during the episode, respectively. The $PM_{2.5}$ contributions in Jilin and Shaanxi provinces are also appreciable, with an average of 9.6 and 6.5 μg m^{-3}, respectively. The average percentage contributions of the NCP emissions to the $PM_{2.5}$ level in Liaoning, Jilin, Shanxi, Shaanxi provinces are 40.6%, 27.5%, 32.2%, and 20.9%, respectively. The NCP emissions contribute remarkably to the O_3 level in Liaoning province, with an average of 46.5 μg m^{-3}, varying from 23.9 to 69.5 μg m^{-3}. The O_3 level in Shanxi province is also influenced considerably by the NCP emissions, with an average contribution of 35.1 μg m^{-3}. The O_3 level in Shanxi province is also influenced considerably by the NCP emissions, with an average contribution of 35.1 μg m^{-3}. The average O_3 contributions of the NCP emissions to Jilin and Shaanxi provinces are 28.7 and 20.7 μg m^{-3}, respectively. The average percentage contributions of the NCP emissions to the afternoon O_3 level in Liaoning, Jilin, Shanxi, and Shaanxi provinces are 27.4%, 19.5%, 21.2%, and 15.8%, respectively. However, the effect of the NCP emissions on the air quality in Inner Mongolia is generally insignificant. Therefore, effective mitigations of the NCP emissions not only improve the local air quality, but also are beneficial to the air quality in the Northeast and Northwest China during the Asian summer monsoon season.

1 Introduction

With the rapid growth of industrialization, urbanization and transportation, China has experienced severe air pollution with high levels of fine particulate matters ($PM_{2.5}$) and ozone (O_3) recently (e.g., Chan and Yao, 2008; Zhang et al., 2013; Kurokawa et al., 2013; Li et al., 2017b). Although the Chinese State Council has issued the 'Atmospheric Pollution Prevention and Control Action Plan' in September 2013 with the aim of improving China's air quality, heavy haze or photochemical smog still frequently plagues China, especially in the North China Plain (NCP)， Yangtze River Delta (YRD), and Pearl River Delta (PRD). Elevated O_3 and $PM_{2.5}$ concentrations in the atmosphere not only perturb regional and global climates, also exert adverse effects on air quality, ecosystems, and human health (Weinhold, 2008; Parrish and Zhu, 2009).

The NCP has become one of the most polluted areas in the world due to a large amount of emissions of pollutants and frequent occurrence of unfavorable meteorological situations, as well as the topography (e.g., Tang et al., 2012; Zhang et al., 2013; Zhuang et al., 2014; Pu et al., 2015; Long et al., 2016). Heavy haze with extremely high $PM_{2.5}$ concentrations often covers the NCP during wintertime, partially attributable to the coal combustion for domestic heating (e.g., He et al., 2001; Cao et al., 2007; H. Li et al., 2017a). However, even in summer, with improvement of the evacuation condition and increase of precipitation, photochemical smog with high levels of $PM_{2.5}$ and O_3 still engulfs the NCP (e.g., Gao et al., 2011; Hu et al., 2014; Cao et al., 2015; Wu et al., 2017). The $PM_{2.5}$ concentrations during summertime in the NCP are generally lower than those in winter, but still much higher than 35 μg m^{-3}, the first grade of National Ambient Air Quality Standards (NAAQS) in China (Feng et al., 2016; Z. S. Wang et al., 2016; Sun et al., 2016). The average summertime $PM_{2.5}$ concentrations in the NCP are 77.0 ± 41.9 μg m^{-3} in 2013, much more than those in other regions of China and also exceeding the second grade of NAAQS (Hu et al., 2014). In addition, increasing O_3

precursors emissions has caused serious O_3 pollution during summertime in the NCP (e.g., Zhang et al., 2009; Xu et al., 2011; Kurokawa et al., 2013). Li et al. (2017b) have reported that the maximum 1h O_3 concentration exceeds 200 μg m^{-3} in almost all the cities in Eastern China from April to September 2015, mainly concentrated in the NCP and YRD, showing a widespread and persistent O_3 pollution. Ma et al. (2016) have found a growth trend of the surface O_3 at a rural site in the NCP from 2003 to 2015, with an average rate of 1.13 ppb per year. Wu et al. (2017) have shown that the average afternoon O_3 concentration in the summer of 2015 in Beijing is about 163 μg m^{-3}.

China is located in a large monsoon domain, and the Asia summer monsoon (ASM) tends to substantially influence the distribution and trans-boundary transport of air pollutants in China. Zhu et al. (2004) have proposed that the summertime high O_3 concentration over Western China is due to the monsoonal transport from Eastern China and long-range transport from South/central Asia and even Europe. Zhao et al. (2010) have also indicated that O_3 transported from South/Central Asia to Western China increases from May to August because of the northward movement of the India summer monsoon. Huang et al. (2015) have suggested that an earlier onset of the ASM would lead to more O_3 enhancement in the lower troposphere over the NCP in later spring and early summer. Numerous studies have also reported that the strength and tempo-spatial extension of the ASM influences the spatial and temporal distribution of aerosol mass concentrations over Eastern China (Cao et al., 2015; Li et al., 2016; Cheng et al., 2016). For example, Zhang et al. (2010) have emphasized that the East ASM plays a major role in determining the seasonal and interannual variations of the $PM_{2.5}$ concentration over Eastern China. Using the GEOS-CHEM model, Zhu et al. (2012) have shown that the weakening of the ASM increases the aerosol concentration in Eastern China. Wu et al. (2016) have pointed out that the regional transport and tempo-spatial distribution of air pollutants are directly influenced by the East Asian monsoon at seasonal,

inter-annual, and decadal scales.

During the ASM season, meteorological conditions are characterized by prevailing southwesterly-southeasterly winds over Eastern China. Air pollutants originated from the NCP are likely to be transported northwards and affect the air quality in its downwind areas, so it is imperative to quantitatively evaluate the effect of the NCP emissions on the air quality in its neighboring regions. Previous studies have concentrated on the composition, characteristics, and sources of the air pollutants over the NCP (e.g., Han et al., 2006; Liu et al., 2012; Zhao et al., 2013; Li et al., 2015). However, few studies have been performed to investigate the effect of trans-boundary transport of air pollutants originated from the NCP on the air quality in the Northeast and Northwest China under the prevailing southerly wind associated with the ASM.

In this study, we first analyze the role of synoptic situations during the ASM (from May to September) in the trans-boundary transport over Northern China and further evaluate the contribution of trans-boundary transport of pollutants originated from the NCP to the air quality in the Northeast and Northwest China using the WRF-CHEM model. The model configuration and methodology are described in Section 2. Analysis results and discussions are presented in Section 3, and conclusions are given in Section 4.

2 Model and Methodology

2.1 WRF-CHEM Model and Configuration

A persistent air pollution episode with high levels of $PM_{2.5}$ and O_3 from 22 to 28 May 2015 in Northern China is simulated using the WRF-CHEM model which is developed by Li et al. (2010, 2011a, b, 2012) at the Molina Center for Energy and the Environment. Table 1 provides detailed model configurations and Figure 1 shows the WRF-CHEM model simulation domain. It is worth noting that the horizontal resolution of 10 km adopted in this

115 study is the lower bound for the WRF model to turn on the cumulus scheme, so the new
116 Kain-Fritch scheme is used in the present study (Table 1). Further description of the model is
117 presented in Supplementary Information (SI).

118 The key characteristics of the aerosol pollution in China are frequently associated with
119 rather efficient secondary formation, including aerosol nucleation and rapid growth under
120 favorable conditions (Zhang et al., 2012; Qiu et al., 2013; Guo et al., 2014; Zhang et al.,
121 2015). The new particle production rate in the WRF-CHEM model is calculated due to the
122 binary nucleation of H_2SO_4 and H_2O vapor. The nucleation rate is a parameterized function
123 of temperature, relative humidity, and the vapor-phase H_2SO_4 concentration, following the
124 work of Kulmala et al. (1998), and the new particles are assumed to be 2.0 nm diameter.
125 Recent studies have shown that organic vapors are involved in the nucleation process (Zhang
126 et al., 2012) and further studies need to be conducted to consider the contributions of organic
127 vapors to the nucleation process. The secondary organic aerosol (SOA) formation is
128 simulated using a non-traditional SOA model including the volatility basis-set modeling
129 method in which primary organic components are assumed to be semi-volatile and
130 photochemically reactive and are distributed in logarithmically spaced volatility bins (Li et al.,
131 2011a). The contributions of glyoxal and methylglyoxal to the SOA formation are also
132 included in the SOA module. The SOA formation from glyoxal and methylglyoxal is
133 parameterized as a first-order irreversible uptake by aerosol particles, with a reactive uptake
134 coefficient of 3.7×10^{-3} for glyoxal and methylglyoxal (Zhao et al., 2006). The simulation of
135 inorganic aerosols in the WRF-CHEM model adopts the ISORROPIA Version 1.7 (Nenes et
136 al., 1998).

137 For the discussion convenience, Northern China is divided into 3 regions (Figure S1): 1)
138 the North China Plain (including Beijing, Tianjin, Hebei, Shandong, Henan, the south of
139 Jiangsu and Anhui, hereafter referred to as the NCP), 2) the Northeast China (including

Heilongjiang, Jilin, Liaoning and the east part of Inner Mongolia, hereafter referred to as the NEC), and 3) the Northwest China (including Shanxi, Shaanxi and the west part of Inner Mongolia, hereafter referred to as the NWC). During the episode, the observed average daily $PM_{2.5}$ concentration was 75.5 μg m^{-3} and the mean O_3 concentration in the afternoon was 151.2 μg m^{-3} in the NCP. Figure S2 presents the distributions of the anthropogenic emission rates of volatile organic compounds (VOCs), nitrogen oxide (NO_x), organic carbon (OC), and SO_2 in Mainland China, showing that the high emission rates of VOCs, NO_x, OC, and SO_2 are generally concentrated in the NCP. It is worth noting that uncertainties in the emission inventory used in this study are rather large considering the rapid changes in anthropogenic emissions that are not fully reflected in the current emission inventory and the complexity of pollutants precursors.

2.2 Data and Methodology

In the present study, the model performance is validated using the hourly measurements of O_3, NO_2, and $PM_{2.5}$ concentrations released by the China's Ministry of Environment Protection (China MEP), which can be accessed at http://www.aqistudy.cn/. In addition, the simulated submicron sulfate, nitrate, ammonium, and organic aerosols are compared to the measurements by the Aerodyne Aerosol Chemical Speciation Monitor (ACSM), which was deployed at the National Center for Nanoscience and Technology (NCNST), Chinese Academy of Sciences in Beijing (Figure 1). The observed mass spectra of organic aerosols are analyzed using the Positive Matrix Factorization (PMF) technique and four components are identified: hydrocarbon-like organic aerosol (HOA)，cooking organic aerosol (COA)，coal combustion organic aerosol (CCOA), and oxygenated organic aerosol (OOA). HOA, COA, and CCOA are interpreted as a surrogate of primary organic aerosols (POA), and OOA is a surrogate of secondary organic aerosols (SOA). Furthermore, the reanalysis data from the

European Centre for Medium-Range Weather Forecasts (ECMWF) are used to analyze the synoptic patterns during the ASM season from May to September 2015.

The mean bias (*MB*), root mean square error (*RMSE*) and the index of agreement (*IOA*) are utilized to evaluate the performance of the WRF-CHEM model simulations against measurements. To assess the contributions of the NCP emissions to the near-surface concentrations of O_3 and $PM_{2.5}$ in the NEC and NWC, the factor separation approach (FSA) is used in this study (Stein and Alpert, 1993; Gabusi et al., 2008; Li et al., 2014). The detailed description of methodology can be found in SI-2.

3 Results and Discussion

3.1 Synoptic Patterns during the ASM Season

The ASM commences to prevail from May to September each year in China, with strong winds blowing from oceans to Eastern China and bringing warm and moist airflow to the continent. Furthermore, the Western Pacific subtropical high gradually intensifies, and moves from south to north to influence the weather and climate over China, also transporting water vapor from the sea to Eastern China. During the ASM season, due to the influence of the Western Pacific subtropical high, rain belts and associated deep convections move from Southeastern China to Northern China (Ding et al., 1992, 2005; Lau et al., 1988, 1992; Kang et al., 2002). Figure 2 shows the geopotential heights at 500 hPa and mean sea level pressure with wind vectors during the ASM season in 2015. At 500 hPa, the main part of subtropical high, which is represented by the scope of the contour of 5880 geopotential meter, is located in Northwest Pacific Ocean. The mean ridgeline of the Western Pacific subtropical high is located at 25°N, moving from south to north from May to September, which substantially affects the synoptic conditions in China. Flat westerly wind at 500 hPa prevails over the NCP and its surrounding regions, indicating a stable weather condition. The mean sea level

pressure shows that most of areas in the NCP are continually influenced by the ASM and the high-pressure system centering in the Western Pacific, causing the prevailing southeasterly - southwesterly wind over the NCP and its surrounding areas. The detailed description of the synoptic conditions during the study episode can be found in SI.

In the region controlled by the Western Pacific subtropical high, a subsidence airflow is dominant with calm or weak winds, and the temperature is extremely high due to the strong sunlight, which is favorable for the accumulation and formation of air pollutants. The air pollutants are likely to be transported from south to north under the persistent effect of southerly winds.

Figures 3 and 4 present the relationship of $PM_{2.5}$ and O_3 concentrations in the NCP with those in the NEC and NWC during the ASM season from 2013 to 2016, respectively. The observed $PM_{2.5}$ and O_3 concentrations in the NCP exhibit a positive correlation with those in the NEC and NWC, with the correlation coefficients generally exceeding 0.55. There are two possible reasons for the positive correlation of $PM_{2.5}$ and O_3 concentrations between the NCP and its surrounding regions. One is that when the NCP and its neighboring areas are controlled by the same large-scale synoptic pattern, the concentrations of air pollutants generally vary synchronously. The other is the trans-boundary transport of air pollutants originated from the NCP to its surrounding areas due to the southerly wind associated with the ASM. The correlation coefficients of $PM_{2.5}$ and O_3 concentrations in the provinces of the NEC with those in the NCP generally decrease from south to north, with the coefficients of 0.69, 0.56 and 0.52 for $PM_{2.5}$, and of 0.86, 0.76, and 0.76 for O_3 in Liaoning, Jilin and Heilongjiang, respectively. The decreasing trend of the correlation coefficients also exists from east to west in the NWC, with coefficients of 0.69 and 0.62 for $PM_{2.5}$, and 0.87 and 0.84 for O_3 in Shanxi and Shaanxi, respectively. Hence, when severe air pollution occurs in the NCP in summer, the air quality in its adjacent provinces is likely to be deteriorated, possibly

214 caused by the trans-boundary transport of air pollutants originated from the NCP.

215 It is worth noting that the intensity of ASM substantially influences the temporal
216 variation and spatial distribution of air pollutants (Wu et al., 2016). The East Asia summer
217 monsoon index proposed by Zhang et al. (2003) is defined as a difference of anomalous zonal
218 wind between the (10°-20°N, 100°-150°E) and (25°-35°N, 100°-150°E) at 850hPa during
219 summer (June-August). The year of monsoon index greater than or equal to 2 is defined as
220 the strong summer monsoon year, and the year of monsoon index less than or equal to -2 is
221 defined as the weak summer monsoon year. The monsoon index calculated by China
222 Meteorological Administration shows that the intensity of the summer monsoon in 2015 is
223 close to the normals (SI-Figure S5).

224 **3.2 Model performance**

225 **3.2.1 $PM_{2.5}$, O_3 and NO_2 Simulations in Northern China**

226 Figure 5 shows the temporal variations of observed and simulated near-surface $PM_{2.5}$,
227 O_3 and NO_2 concentrations averaged over monitoring sites in Northern China. The
228 WRF-CHEM model generally simulates well the diurnal variation of $PM_{2.5}$ concentrations in
229 Northern China, with *IOA* of 0.91. The model successfully reproduces the temporal variations
230 of surface O_3 concentrations compared with observations in Northern China, e.g., peak O_3
231 concentrations in the afternoon due to active photochemistry and low O_3 concentrations
232 during nighttime caused by the NO_x titration, with *IOA* of 0.98. However, the model
233 underestimation still exists in simulating the O_3 concentration, with a *MB* of -4.0 μg m^{-3}. The
234 model also reasonably yields the NO_2 diurnal profiles, but frequently overestimates the NO_2
235 concentrations in the late evening due to the simulated low PBL height, and underestimates
236 the concentration in the early morning because of the uncertainties in the NO_x emissions. The
237 further analysis of the model performance of $PM_{2.5}$, O_3 and NO_2 concentrations in Northern
238 China can be found in SI.

3.2.2 Aerosol Species Simulations in Beijing

Figure 6 presents the temporal variations of simulated and observed aerosol species at NCNST site in Beijing from 22 to 28 May 2015. Generally, the WRF-CHEM model predicts reasonably the temporal variations of the aerosol species against the measurements, especially for POA and nitrate aerosol, with *IOA*s of 0.81 and 0.90, respectively. The model has difficulties in well simulating the SOA concentrations, with the *IOA* and *MB* of 0.69 and -3.6 μg m^{-3}, respectively. It is worth noting that many factors influence the SOA simulation, including measurements, meteorology, precursors emissions, SOA formation mechanisms and treatments (Bei et al., 2012, 2013). The model reasonably tracks the temporal variation of the observed sulfate concentration, but the bias is still large, and the *MB* and *IOA* are -1.2 μg m^{-3} and 0.68, respectively. The sulfate source in the atmosphere is various, including SO_2 gas-phase oxidations by hydroxyl radicals (OH) and stabilized criegee intermediates (sCI), aqueous reactions in cloud or fog droplets, and heterogeneous reactions on aerosol surfaces, as well as direct emissions from power plants and industries (G. H. Li et al., 2017a). G. Wang et al. (2016) have also reported that the aqueous oxidation of SO_2 by NO_2 is important to the efficient sulfate formation. Considering that the model fails to well resolve convective clouds due to the 10km horizontal resolution, the sulfate formation from the cloud process is generally underestimated. Additionally, large amount of SO_2 is emitted from point sources, such as power plants or agglomerated industrial zones, which is much more sensitive to wind fields simulations (Bei et al., 2010). The model performs reasonably well in simulating the ammonium aerosol, with the *IOA* and *MB* of 0.77 and -0.4 μg m^{-3}, respectively.

3.2.3 Simulations of the Spatial Distribution of $PM_{2.5}$ and O_3 Concentrations

The peak $PM_{2.5}$ concentration generally occurs from 08:00 to 10:00 Beijing Time (BJT) due to the rush hour. Figure 7 provides the distributions of calculated and observed near-surface $PM_{2.5}$ concentrations along with the simulated wind fields at 08:00 BJT from 23

to 28 May 2015. The calculated $PM_{2.5}$ spatial patterns generally agree well with the observations at the monitoring sites. The NCP experiences severer $PM_{2.5}$ pollution than its surrounding areas, with $PM_{2.5}$ concentrations frequently exceeding 150 μg m^{-3} in the Beijing-Tianjin-Hebei region. During the study episodes, the pollutants are likely to be transported to the NEC and NWC under the prevailing southwesterly or southeasterly winds in Northern China, causing the $PM_{2.5}$ concentrations in most of areas of the NEC and NWC frequently to be higher than 75 μg m^{-3}.

The O_3 concentration during summertime generally reaches its peak from 14:00 to 16:00 BJT in Northern China (Figure 5). Figure 8 shows the spatial distribution of calculated and measured near-surface O_3 concentrations at 14:00 BJT from 23 to 28 May 2015, along with the simulated wind fields. Generally, the simulated O_3 spatial patterns are consistent with the observations, but the model overestimation or underestimation still exists. The simulated high O_3 concentrations at 14:00 BJT, exceeding 200 μg m^{-3}, are frequently concentrated in the NCP, which is also consistent with the measurements. The O_3 transport to the NEC and NWC from the NCP is obvious when the winds are southeasterly or southwesterly, inducing the severe O_3 pollution in the NEC and NWC.

In general, the simulated variations of $PM_{2.5}$, O_3, NO_2 and aerosol species are in good agreement with observations, indicating that the simulations of meteorological conditions, chemical processes and the emission inventory used in the WRF-CHEM model are reasonable, providing a reliable base for the further investigation.

3.3 Effects of the NCP Emissions on the Air Quality in the NEC and NWC

To evaluate the contribution of the NCP emissions to the air quality in its neighboring areas, four model simulations are performed, including $\boldsymbol{f_{NS}}$ with all anthropogenic emissions from the NCP and non-NCP areas, $\boldsymbol{f_N}$ with anthropogenic emissions from the NCP only, $\boldsymbol{f_S}$ with anthropogenic emissions from the non-NCP areas only, and $\boldsymbol{f_0}$ without

289 all anthropogenic emissions. Consequently, the air pollutants concentrations in the NEC and
290 NWC can be separated into four components, including contributions from the local
291 emissions (f'_S, $f_S - f_0$), the trans-boundary transport of the NCP emissions (f'_N, $f_N - f_0$),
292 the interactions of these two emissions (f'_{NS}, $f_{NS} - f_N - f_S + f_0$) and the background
293 (f_0).

294 In the present study, the effect of the NCP emissions on the $PM_{2.5}$ and O_3 concentrations
295 in the NEC and NWC is evaluated, considering that they have the long lifetime of several
296 days in the troposphere and often constitute the primary air pollutant during summertime
297 (Seinfeld and Pandis, 2006). However, the trans-boundary transport of PM_{10} is not considered
298 due to its short lifetime of several hours caused by the dry deposition and gravity and the fact
299 that PM_{10} is generally confined to its source region when the wind is not strong enough (Sun
300 et al., 2006).

301 **3.3.1 Contributions of the NCP Emissions to $PM_{2.5}$ Levels in the NEC and NWC**

302 Figure 9 shows the simulated spatial distribution of daily mean $PM_{2.5}$ concentrations
303 contributed by the NCP emissions in the NEC and NWC from 23 to 28 May 2015. The
304 contribution of trans-boundary transport of the NCP emissions to the $PM_{2.5}$ concentration is
305 remarkable in Liaoning, frequently exceeding 30 μg m^{-3} in most areas of the province during
306 the episode. The NCP emissions also considerably influence the $PM_{2.5}$ concentration in Jilin,
307 contributing 5~30 μg m^{-3} in most areas and occasionally exceeding 40 μg m^{-3}. The effect of
308 the NCP emissions on the $PM_{2.5}$ level in Shanxi and Shaanxi is increasingly evident from 23
309 to 28 May 2015, with the contribution of up to 50~60 μg m^{-3} in southeast of Shanxi and to a
310 lesser extent of 30~40 μg m^{-3} in the middle part of Shaanxi on 27- 28 May. The contribution
311 of trans-boundary transport of the NCP emissions to the $PM_{2.5}$ level in Inner Mongolia is not
312 significant, which may be attributed to the location of the low pressure and terrain
313 characteristics. Obviously, the effect of trans-boundary transport shows a stepwise

characteristic: the closer to the NCP emission sources, the more remarkable the impact on the downwind areas. As a result, Liaoning and Shanxi provinces are substantially influenced by the NCP emissions, while Jilin and Shaanxi provinces are affected to a lesser extent.

The impact of the NCP emissions on the daily average $PM_{2.5}$ concentration in the NEC and NWC from 22 to 28 May 2015 is summarized in Table 2. On average, the NCP emissions increase the $PM_{2.5}$ concentrations by 24.2, 9.6, 13.9, 6.5, and 2.6 μg m^{-3} in Liaoning, Jilin, Shanxi, Shaanxi, and Inner Mongolia, with the average percentage contribution of 40.6%, 27.5%, 32.2%, 20.9%, and 16.7%, respectively. Figure 10 shows the episode-averaged $PM_{2.5}$ percentage contribution from the NCP emissions to the surrounding areas. The NCP emissions markedly affect the air quality in Liaoning, accounting for around 20%-50% of the $PM_{2.5}$ concentration during the episode and with the most substantial impact on the west part of the province. The NCP emissions contribute about 15%-30% of the $PM_{2.5}$ concentration in Jilin. Shanxi province is also remarkably affected by the NCP emissions, with more than 25% of $PM_{2.5}$ concentration contributed by the NCP emissions in most areas. Although Shaanxi province is a little far from the NCP, the NCP emissions still contribute about 10%-35% of the $PM_{2.5}$ concentration. The NCP emissions also enhance the $PM_{2.5}$ concentration by 5-50% in the southern edge of Inner Mongolia, which is adjacent to the NCP.

3.3.2 Contributions of the NCP Emissions to O_3 Concentrations in the NEC and NWC

Figure 11 shows the simulated spatial distribution of the average afternoon O_3 concentrations contributed by the NCP emissions from 23 to 28 May 2015. Similar to the $PM_{2.5}$ case, the contribution of the NCP emissions to the O_3 formation in Liaoning and Jilin province is increasingly enhanced during the episode (except on 26 May), and on 25 and 27 May, the NCP emissions account for more than 70 μg m^{-3} of the O_3 concentration in most areas of Liaoning. On 25 and 28 May, the NCP emissions contribute more than 70 μg m^{-3} of the O_3 concentration in some regions of Jilin. A less impact of the NCP emissions on Jilin

339 province on 26 May is due to the weakening of the low pressure. The NCP emissions play a
340 progressively important role in O_3 concentrations in Shanxi and Shaanxi provinces during the
341 episode, especially on 27 and 28 May when the contribution can be up to 60 μg m^{-3}. The
342 impact of the NCP emissions on O_3 concentrations in Inner Mongolia is insignificant overall.
343 Table 3 summarizes the effects of the NCP emissions on the average afternoon O_3
344 concentration in the NEC and NWC from 22 to 28 May 2015. During the episode, the NCP
345 emissions substantially influence the O_3 level in Liaoning province, and the afternoon O_3
346 contribution is about 46.5 μg m^{-3} on average, ranging from 23.9 to 69.5 μg m^{-3}. The NCP
347 emissions also contribute an average of 28.7 μg m^{-3} to the O_3 concentration in Jilin province,
348 varying from 12.4 to 45.7 μg m^{-3}. The contribution of NCP emissions to Shanxi and Shanxi
349 provinces becomes increasingly significant during the episode, with an average of 35.1 μg
350 m^{-3} for Shanxi province and 20.7 μg m^{-3} for Shaanxi province, respectively. The O_3
351 concentration in Inner Mongolia is less influenced by the NCP emissions, with an average of
352 8.4 μg m^{-3}. Figure 12 illustrates the episode-averaged afternoon O_3 percentage contribution of
353 the NCP emissions to the surrounding areas. In the NEC, the NCP emissions account for
354 15-35% of the afternoon O_3 concentration in most areas of Liaoning province, and 10-30% in
355 Jilin province. In the NWC, the NCP emissions contribute 10-35% of the O_3 concentration in
356 Shanxi province, and 10-25% in Shaanxi. In Inner Mongolia, the impact of the NCP
357 emissions on O_3 formation is small, generally less than 15% except in the southern area
358 adjacent to the NCP and Liaoning province where a contribution of more than 10% is found.
359 On average, the NCP emissions distinctly increase the afternoon O_3 concentrations in
360 Liaoning, Jilin, Shanxi, Shaanxi, and Inner Mongolia, with the average percentage of 27.4%,
361 19.5%, 21.2%, 15.8%, and 8.0%, respectively (Table 3).
362 Additional sensitivity studies have also been performed to examine the potential
363 influences of the cumulus parameterization on evaluation of the contribution of the NCP

emissions to the $PM_{2.5}$ and O_3 concentrations in the NEC and NWC, in which the cumulus parameterization is turned off. The difference of the contribution of NCP emissions to the $PM_{2.5}$ and O_3 concentrations in the NEC and NWC is less than 0.8% between the simulations with and without the cumulus parameterization. Furthermore, it is worth noting that uncertainties from meteorological field simulations, emission inventories, and the chemical mechanism used in simulations, have large potentials to influence evaluation of the effect of the NCP emissions on the $PM_{2.5}$ and O_3 concentrations in the NEC and NWC (Carter and Atkinson, 1996; Lei et al., 2004; Song et al., 2009; Bei et al., 2017).

4 Summary and Conclusions

Analyses of the synoptic pattern during the ASM season show that the southeasterly-southwesterly winds prevail in Northern China, facilitating the trans-boundary transport of air pollutants from the NCP to the NEC and NWC. The good relationships of $PM_{2.5}$ and O_3 concentrations in the NCP with those in the NEC and NWC during the ASM season also indicate the possibility that the air quality in the NEC and NWC is influenced by the trans-boundary transport of air pollutants originated from the NCP.

A widespread and severe pollution episode from 22 to 28 May 2015 in Northern China is further simulated using the WRF-CHEM model to investigate the impact of trans-boundary transport of the NCP emissions on $PM_{2.5}$ and O_3 concentrations in the NEC and NWC, when the region is affected by prevailing southeasterly-southwesterly winds associated with the ASM.

In general, the WRF-CHEM model well reproduces the temporal variations and spatial distributions of $PM_{2.5}$, O_3, and NO_2 concentrations compared to observations in Northern China, although the model biases still exist due to the uncertainties in simulated meteorological fields and the emission inventory. The model also performs reasonably well in

simulating the variations of aerosol constituents against the ACSM measurement at the NCNST site in Beijing.

The FSA method is used to investigate the contribution of trans-boundary transport of the NCP emissions to O_3 and $PM_{2.5}$ levels in the NEC and NWC. Model results show that the NCP emissions contribute approximately an average of 24.2 and 13.9 μg m^{-3} to the $PM_{2.5}$ concentration in Liaoning and Shanxi during the episode, with the average percentage contribution of 40.6% and 32.2%, respectively. The NCP emissions enhance the $PM_{2.5}$ level by 9.6 and 6.5 μg m^{-3} in Jilin and Shaanxi on average, with the percentage contribution of 27.5% and 20.9%, respectively. The NCP emissions also substantially influence the O_3 concentration in the NEC and NWC. The NCP emissions increase the afternoon (12:00 - 18:00 BJT) O_3 concentration in Liaoning by 46.5 μg m^{-3} on average during the episode, followed by 35.1 μg m^{-3} in Shanxi, 28.7 μg m^{-3} in Jilin, and 20.7 μg m^{-3} in Shaanxi, with the average percentage contribution of 27.4%, 21.2%, 19.5%, and 15.8%, respectively. In contrast, the contribution of trans-boundary transport of the NCP emissions to the $PM_{2.5}$ and O_3 concentration in Inner Mongolia are less, with an average of 2.6 and 8.4 μg m^{-3}, respectively. Our results demonstrate that when southerly winds are prevailing in Northern China, air pollutants originated from the NCP are likely to be transported northwards and profoundly affect the air quality in the NEC and NWC. Stringent control of the NCP emissions not only mitigates the local air pollution, also is beneficial to the air quality in the NEC and NWC during the ASM season.

It is worth noting that interactions between the air pollution in China and ASM are two-way and their relationships are complicated and interrelated, especially with regard to the aerosol-meteorology interaction. Aerosol impacts on meteorology is significant due to its direct and indirect effects, which further influence the air pollution condition in the lower troposphere. Aerosol semi-direct effect induced by the light absorbing aerosols in the

atmosphere stabilizes planetary boundary layer (PBL) and thus reduces the PBL height to exacerbate accumulation of air pollutants within the PBL, particularly for the aging process of black carbon which considerably enhances light absorption (Wang et al., 2013; Khalizov et al., 2009; Peng et al., 2016). In addition, aerosol plays an important role in the process of cloud formation and precipitation via acting as cloud condensation nuclei (CCN) and ice nuclei (IC). Therefore, aerosol-cloud interactions modify temperature and moisture profiles and influence precipitation, leading to potential feedback on the atmospheric chemistry (Wang et al., 2011). In addition, the ASM substantially influence spatial characteristics of the air pollutants transport and distribution in Eastern China on seasonal, inter-annual, and decadal scales (Wu et al., 2016). Further studies need to be performed to investigate the impacts of the ASM variation on the air pollutants transport, which is modulated by climate changes.

Although the model performs well in simulating $PM_{2.5,}$ O_3 and NO_2 during the episode in northern China, the uncertainties from meteorological fields and the emission inventory still exist. Future studies need to be conducted to improve the WRF-CHEM model simulations, and to further assess the contributions of trans-boundary transport of the NCP emissions under specific synoptic patterns, considering the rapid changes in anthropogenic emissions, which is not reflected in the present study. Therefore, more episode simulations during the ASM season should be performed to comprehensively evaluate the contribution of trans-boundary transport of the NCP emissions to the air quality in its downwind regions and support the design and implementation of effective emission control strategies.

Acknowledgements. This work is financially supported by the National Key R&D Plan (Quantitative Relationship and Regulation Principle between Regional Oxidation Capacity of Atmospheric and Air Quality (2017YFC0210000)). Naifang Bei is supported by the National Natural Science Foundation of China (no. 41275101 and no. 41430424) and the Fundamental Research Funds for the Central Universities of China. Guohui Li is supported by the Hundred Talents Program of the Chinese Academy of Sciences and the National Natural Science Foundation of China (no. 41661144020).

Reference

Bei, N., Lei, W., Zavala, M., and Molina, L. T.: Ozone predictabilities due to meteorological uncertainties in the Mexico City basin using ensemble forecasts, Atmospheric Chemistry and Physics, 10, 6295-6309, 10.5194/acp-10-6295-2010, 2010.

Bei, N., Li, G., and Molina, L. T.: Uncertainties in SOA simulations due to meteorological uncertainties in Mexico City during MILAGRO-2006 field campaign, Atmospheric Chemistry and Physics, 12, 11295-11308, 10.5194/acp-12-11295-2012, 2012.

Bei, N. F., Li, G. H., Zavala, M., Barrera, H., Torres, R., Grutter, M., Gutierrez, W., Garcia, M., Ruiz-Suarez, L. G., Ortinez, A., Guitierrez, Y., Alvarado, C., Flores, I., and Molina, L. T.: Meteorological overview and plume transport patterns during Cal-Mex 2010, Atmospheric Environment, 70, 477-489, 10.1016/j.atmosenv.2012.01.065, 2013.

Bei, N. F., Wu, J. R., Elser, M., Feng, T., Cao, J. J., El-Haddad, I., Li, X., Huang, R. J., Li, Z. Q., Long, X., Xing, L., Zhao, S. Y., Tie, X. X., Prevot, A. S. H., and Li, G. H.: Impacts of meteorological uncertainties on the haze formation in Beijing-Tianjin-Hebei (BTH) during wintertime: a case study, Atmospheric Chemistry and Physics, 17, 14579-14591, 10.5194/acp-17-14579-2017, 2017.

Cao, Z. Q., Sheng, L. F., Liu, Q., Yao, X. H., and Wang, W. C.: Interannual increase of regional haze-fog in North China Plain in summer by intensified easterly winds and orographic forcing, Atmospheric Environment, 122, 154-162, 10.1016/j.atmosenv.2015.09.042, 2015.

Cao, J. J., Lee, S. C., Chow, J. C., Watson, J. G., Ho, K. F., Zhang, R. J., Jin, Z. D., Shen, Z. X., Chen, G. C., and Kang, Y. M.: Spatial and seasonal distributions of carbonaceous aerosols over China, Journal of Geophysical Research Atmospheres, 112, 22-11, 2007.

Carter, W. P. L., and Atkinson, R.: Development and evaluation of a detailed mechanism for the atmospheric reactions of isoprene and NO_x, International Journal of Chemical Kinetics, 28, 497-530, 1996.

Chan, C. K., and Yao, X.: Air pollution in mega cities in China, Atmospheric Environment, 42, 1-42, 2008.

Chen, F., and Dudhia, J.: Coupling an advanced land surface-hydrology model with the Penn State-NCAR MM5 modeling system. Part I: Model implementation and sensitivity, Monthly Weather Review, 129, 569-585, 10.1175/1520-0493(2001)129<0569:caalsh>2.0.co;2, 2001.

Cheng, X. G., Zhao, T. L., Gong, S. L., Xu, X. D., Han, Y. X., Yin, Y., Tang, L. L., He, H. C., and He, J. H.: Implications of East Asian summer and winter monsoons for interannual aerosol variations over central-eastern China, Atmospheric Environment, 129, 218-228, 10.1016/j.atmosenv.2016.01.037, 2016.

Chou, M. D., and Suarez, M. J.: A solar radiation parameterization for atmospheric studies, NASA TM-104606, Nasa Tech.memo, 15, 1999.

Chou, M. D., Suarez, M. J., Liang, X. Z., Yan, M. H., and Cote, C.: A Thermal Infrared Radiation Parameterization for Atmospheric Studies, Max J, 2001.

Ding, Y. H.: Summer monsoon rainfalls in china, Journal of Meteorological Society of Japan, 70, 373-396, 1992.

Ding, Y. H., and Chan, J. C. L.: The East Asian summer monsoon: an overview, Meteorology and Atmospheric Physics, 89, 117-142, 10.1007/s00703-005-0125-z, 2005.

Feng, T., Bei, N. F., Huang, R. J., Cao, J. J., Zhang, Q., Zhou, W. J., Tie, X. X., Liu, S. X., Zhang, T., Su, X. L., Lei, W. F., Molina, L. T., and Li, G. H.: Summertime ozone formation in Xi'an and surrounding areas, China, Atmospheric Chemistry and Physics, 16, 4323-4342, 10.5194/acp-16-4323-2016, 2016.

Gabusi, V., Pisoni, E., and Volta, M.: Factor separation in air quality simulations, Ecological Modelling, 218, 383-392, 10.1016/j.ecolmodel.2008.07.030, 2008.

Gao, Y., Liu, X., Zhao, C., and Zhang, M.: Emission controls versus meteorological conditions in determining aerosol concentrations in Beijing during the 2008 Olympic Games, Atmospheric Chemistry and Physics, 11, 12437-12451, 10.5194/acp-11-12437-2011, 2011.

Guenther, A., Karl, T., Harley, P., Wiedinmyer, C., Palmer, P. I., and Geron, C.: Estimates of global terrestrial isoprene emissions using MEGAN (Model of Emissions of Gases and Aerosols from Nature), Atmospheric Chemistry and Physics, 6, 3181-3210, 2006.

Guo, S., Hu, M., Zamora, M. L., Peng, J. F., Shang, D. J., Zheng, J., Du, Z. F., Wu, Z., Shao, M., Zeng, L. M., Molina, M. J., and Zhang, R. Y.: Elucidating severe urban haze formation in China, Proceedings of the National Academy of Sciences of the United States of America, 111, 17373-17378, 10.1073/pnas.1419604111, 2014.

Han, J. S., Moon, K. J., Lee, S. J., Kim, Y. J., Ryu, S. Y., Cliff, S. S., and Yi, S. M.: Size-resolved source apportionment of ambient particles by positive matrix factorization at Gosan background site in East Asia, Atmospheric Chemistry and Physics, 6, 211-223, 2006.

He, K., Yang, F., Ma, Y., Zhang, Q., Yao, X., Chan, C. K., Cadle, S., Chan, T., and Mulawa, P.: The characteristics of $PM_{2.5}$ in Beijing, China, Atmospheric Environment, 35, 4959-4970, 2001.

Hong, S.-Y., and Lim, J.-O. J.: The WRF Single-Moment 6-Class Microphysics Scheme (WSM6), Asia-Pacific Journal of Atmospheric Sciences, 42, 129-151, 2006.

Horowitz, L. W., Walters, S., Mauzerall, D. L., Emmons, L. K., Rasch, P. J., Granier, C., Tie, X. X., Lamarque, J. F., Schultz, M. G., Tyndall, G. S., Orlando, J. J., and Brasseur, G. P.: A global simulation of tropospheric ozone and related tracers: Description and evaluation of MOZART, version 2, Journal of Geophysical Research-Atmospheres, 108, 29, 10.1029/2002jd002853, 2003.

Hu, J. L., Wang, Y. G., Ying, Q., and Zhang, H. L.: Spatial and temporal variability of $PM_{2.5}$ and PM10 over the North China Plain and the Yangtze River Delta, China, Atmospheric Environment, 95, 598-609, 10.1016/j.atmosenv.2014.07.019, 2014.

Huang, J., Liu, H., Crawford, J. H., Chan, C., Considine, D. B., Zhang, Y., Zheng, X., Zhao, C., Thouret, V., Oltmans, S. J., Liu, S. C., Jones, D. B. A., Steenrod, S. D., and Damon, M. R.: Origin of springtime ozone enhancements in the lower troposphere over Beijing: in situ measurements and model analysis, Atmospheric Chemistry and Physics, 15, 5161-5179, 10.5194/acp-15-5161-2015, 2015.

Janjić, Z. I.: Nonsingular Implementation of the Mellor–Yamada Level 2.5 Scheme in the NCEP Meso Model, Ncep Office Note, 436, 2002.

534 Kang, I. S., Jin, K., Wang, B., Lau, K. M., Shukla, J., Krishnamurthy, V., Schubert, S. D.,
535 Wailser, D. E., Stern, W. F., Kitoh, A., Meehl, G. A., Kanamitsu, M., Galin, V. Y.,
536 Satyan, V., Park, C. K., and Liu, Y.: Intercomparison of the climatological variations of
537 Asian summer monsoon precipitation simulated by 10 GCMs, Climate Dynamics, 19,
538 383-395, 10.1007/s00382-002-0245-9, 2002.

539 Kain, J. S.: The Kain Fritsch Convective Parameterization: An Update, Journal of Applied
540 Meteorology, 43, 170-181, 2004.

541 Khalizov, A. F., Xue, H. X., Wang, L., Zheng, J., and Zhang, R. Y.: Enhanced Light
542 Absorption and Scattering by Carbon Soot Aerosol Internally Mixed with Sulfuric Acid,
543 Journal of Physical Chemistry A, 113, 1066-1074, 10.1021/jp807531n, 2009.

544 Kulmala, M., Laaksonen, A., and Pirjola, L.: Parameterizations for sulfuric acid/water
545 nucleation rates, Journal of Geophysical Research, 103, 8301– 8307, 1998.

546 Kurokawa, J., Ohara, T., Morikawa, T., Hanayama, S., Janssens-Maenhout, G., Fukui, T.,
547 Kawashima, K., and Akimoto, H.: Emissions of air pollutants and greenhouse gases over
548 Asian regions during 2000-2008: Regional Emission inventory in ASia (REAS) version 2,
549 Atmospheric Chemistry and Physics, 13, 11019-11058, 10.5194/acp-13-11019-2013,
550 2013.

551 Lau, K. M., Yang, G. J., and Shen, S. H.: Seasonal and intraseasonal climatology of summer
552 monsoon rainfall over East-Asia, Monthly Weather Review, 116, 18-37,
553 10.1175/1520-0493(1988)116<0018:saicos>2.0.co;2, 1988.

554 Lau, K. M.: East-asian summer monsoon rainfall variability and climate teleconnection,
555 Journal of Meteorological Society of Japan, 70, 211-242, 1992.

556 Lei, W., Zhang, R., Tie, X., and Hess, P.: Chemical characterization of ozone formation in
557 the Houston‐Galveston area: A chemical transport model study, Journal of Geophysical
558 Research Atmospheres, 109, -, 2004.

559 Li, G., Lei, W., Zavala, M., Volkamer, R., Dusanter, S., Stevens, P., and Molina, L. T.:
560 Impacts of HONO sources on the photochemistry in Mexico City during the
561 MCMA-2006/MILAGO Campaign, Atmospheric Chemistry and Physics, 10, 6551-6567,
562 10.5194/acp-10-6551-2010, 2010.

563 Li, G., Bei, N., Tie, X., and Molina, L. T.: Aerosol effects on the photochemistry in Mexico
564 City during MCMA-2006/MILAGRO campaign, Atmospheric Chemistry and Physics, 11,
565 5169-5182, 10.5194/acp-11-5169-2011, 2011a.

566 Li, G., Zavala, M., Lei, W., Tsimpidi, A. P., Karydis, V. A., Pandis, S. N., agaratna, M. R.,
567 and Molina, L. T.: Simulations of organic aerosol concentrations in Mexico City using
568 the WRF-CHEM model during the MCMA-2006/MILAGRO campaign, Atmospheric
569 Chemistry and Physics, 11, 3789-3809, 10.5194/acp-11-3789-2011, 2011b.

570 Li, G., Lei, W., Bei, N., and Molina, L. T.: Contribution of garbage burning to chloride and
571 $PM_{2.5}$ in Mexico City, Atmospheric Chemistry and Physics, 12, 8751-8761,
572 10.5194/acp-12-8751-2012, 2012.

573 Li, G. H., Bei, N. F., Zavala, M., and Molina, L. T.: Ozone formation along the California
574 Mexican border region during Cal-Mex 2010 field campaign, Atmospheric Environment,
575 88, 370-389, 10.1016/j.atmosenv.2013.11.067, 2014.

576 Li, G., Bei, N., Cao, J., Huang, R., Wu, J., Feng, T., Wang, Y., Liu, S., Zhang, Q., and Tie, X.:
577 A possible pathway for rapid growth of sulfate during haze days in China, Atmospheric
578 Chemistry and Physics, 17, 1-43, 2017a.

579 Li, G., Bei, N., Cao, J., Wu, J., Long, X., Feng, T., Dai, W., Liu, S., Zhang, Q., and Tie, X.:
580 Widespread and persistent ozone pollution in eastern China during the non-winter season
581 of 2015: observations and source attributions, Atmospheric Chemistry and Physics, 17,
582 1-39, 2017b.

583 Li, J., Xie, S. D., Zeng, L. M., Li, L. Y., Li, Y. Q., and Wu, R. R.: Characterization of
584 ambient volatile organic compounds and their sources in Beijing, before, during, and after
585 Asia-Pacific Economic Cooperation China 2014, Atmospheric Chemistry and Physics, 15,
586 7945-7959, 10.5194/acp-15-7945-2015, 2015.

587 Li, H., Zhang, Q., Zhang, Q., Chen, C., Wang, L., Wei, Z., Zhou, S., Parworth, C., Zheng, B.,
588 and Canonaco, F.: Wintertime aerosol chemistry and haze evolution in an extremely
589 polluted city of the North China Plain: significant contribution from coal and biomass
590 combustion, Atmospheric Chemistry and Physics, 17, 1-31, 2017a.

591 Li, Z. Q., Lau, W. K. M., Ramanathan, V., Wu, G., Ding, Y., Manoj, M. G., Liu, J., Qian, Y.,
592 Li, J., Zhou, T., Fan, J., Rosenfeld, D., Ming, Y., Wang, Y., Huang, J., Wang, B., Xu, X.,
593 Lee, S. S., Cribb, M., Zhang, F., Yang, X., Zhao, C., Takemura, T., Wang, K., Xia, X.,
594 Yin, Y., Zhang, H., Guo, J., Zhai, P. M., Sugimoto, N., Babu, S. S., and Brasseur, G. P.:
595 Aerosol and monsoon climate interactions over Asia, Reviews of Geophysics, 54,
596 866-929, 10.1002/2015rg000500, 2016.

597 Liu, Z., Wang, Y., Gu, D., Zhao, C., Huey, L. G., Stickel, R., Liao, J., Shao, M., Zhu, T.,
598 Zeng, L., Amoroso, A., Costabile, F., Chang, C. C., and Liu, S. C.: Summertime
599 photochemistry during CAREBeijing-2007: ROx budgets and O_3 formation, Atmospheric
600 Chemistry and Physics, 12, 7737-7752, 10.5194/acp-12-7737-2012, 2012.

601 Long, X., Tie, X. X., Cao, J. J., Huang, R. J., Feng, T., Li, N., Zhao, S. Y., Tian, J., Li, G. H.,
602 and Zhang, Q.: Impact of crop field burning and mountains on heavy haze in the North
603 China Plain: a case study, Atmospheric Chemistry and Physics, 16, 9675-9691,
604 10.5194/acp-16-9675-2016, 2016.

605 Ma, Z., Xu, J., Quan, W., Zhang, Z., Lin, W., and Xu, X.: Significant increase of surface
606 ozone at a rural site, north of eastern China, Atmospheric Chemistry and Physics, 16,
607 3969-3977, 2016.

608 Nenes, A., Pandis, S. N., and Pilinis, C.: ISORROPIA: A new thermodynamic equilibrium
609 model for multiphase multicomponent inorganic aerosols, Aquatic Geochemistry, 4,
610 123-152, 10.1023/a:1009604003981, 1998.

611 Parrish, D. D., and Zhu, T.: Clean Air for Megacities, Science, 326, 674-675,
612 10.1126/science.1176064, 2009.

613 Peng, J. F., Hu, M., Guo, S., Du, Z. F., Zheng, J., Shang, D. J., Zamora, M. L., Zeng, L. M.,
614 Shao, M., Wu, Y. S., Zheng, J., Wang, Y., Glen, C. R., Collins, D. R., Molina, M. J., and
615 Zhang, R. Y.: Markedly enhanced absorption and direct radiative forcing of black carbon
616 under polluted urban environments, Proceedings of the National Academy of Sciences of
617 the United States of America, 113, 4266-4271, 10.1073/pnas.1602310113, 2016.

618 Pu, W. W., Zhao, X. J., Shi, X. F., Ma, Z. Q., Zhang, X. L., and Yu, B.: Impact of long-range
619 transport on aerosol properties at a regional background station in Northern China,

620 Atmospheric Research, 153, 489-499, 10.1016/j.atmosres.2014.10.010, 2015.

621 Qiu, C., and Zhang, R. Y.: Multiphase chemistry of atmospheric amines, Physical Chemistry
622 Chemical Physics, 15, 5738-5752, 10.1039/c3cp43446j, 2013.

623 Seinfeld, J. H. and Pandis, S. N.: Atmospheric Chemistry and Physics: From Air Pollution to
624 Climate Change, 2nd Edn., John Wiley & Sons Inc., New York, 2006.

625 Song, J., Lei, W., Bei, N., Zavala, M., Foy, B. D., Volkamer, R., Cardenas, B., Zheng, J.,
626 Zhang, R., and Molina, L. T.: Ozone response to emission changes: a modeling study
627 during the MCMA-2006/MILAGRO Campaign, Atmospheric Chemistry and Physics
628 Discussions, 9, 3827-3846, 2009.

629 Stein, U., and Alpert, P.: Factor separation in numerical simulations, Journal of the
630 Atmospheric Science, 50, 2107-2115, 10.1175/1520-0469(1993)
631 050<2107:fsins>2.0.co;2, 1993.

632 Sun, Y. L., Zhuang, G. S., Tang, A. H., Wang, Y., and An, Z. S.: Chemical characteristics of
633 $PM_{2.5}$ and PM_{10} in haze-fog episodes in Beijing, Environmental Science and Technology,
634 40, 3148-3155, 10.1021/es051533g, 2006.

635 Sun, Y., Jiang, Q., Xu, Y., Ma, Y., Zhang, Y., Liu, X., Li, W., Wang, F., Li, J., and Wang, P.:
636 Aerosol characterization over the North China Plain: Haze life cycle and biomass burning
637 impacts in summer, Journal of Geophysical Research Atmospheres, 121, n/a-n/a, 2016.

638 Tang, G., Wang, Y., Li, X., Ji, D., Hsu, S., and Gao, X.: Spatial-temporal variations in
639 surface ozone in Northern China as observed during 2009-2010 and possible implications
640 for future air quality control strategies, Atmospheric Chemistry and Physics, 12,
641 2757-2776, 10.5194/acp-12-2757-2012, 2012.

642 Wang, G., Zhang, R., Gomez, M. E., Yang, L., Zamora, M. L., Hu, M., Lin, Y., Peng, J., Guo,
643 S., and Meng, J.: Persistent sulfate formation from London Fog to Chinese haze,
644 Proceedings of the National Academy of Sciences of the United States of America, 113,
645 13630, 2016.

646 Wang, Y., Wan, Q., Meng, W., Liao, F., Tan, H., and Zhang, R.: Long-term impacts of
647 aerosols on precipitation and lightning over the Pearl River Delta megacity area in China,
648 Atmospheric Chemistry and Physics, 11, 12421-12436, 10.5194/acp-11-12421-2011,
649 2011.

650 Wang, Y., Khalizov, A., Levy, M., and Zhang, R. Y.: New Directions: Light absorbing
651 aerosols and their atmospheric impacts, Atmospheric Environment, 81, 713-715,
652 10.1016/j.atmosenv.2013.09.034, 2013.

653 Wang, Z. S., Zhang, D. W., Li, Y. T., Dong, X., Sun, R. W., and Sun, N. D.: Different air
654 pollution situations of O_3 and $PM_{2.5}$ during summer in Beijing, 2016.

655 Weinhold, B.: Ozone nation - EPA standard panned by the people, Environmental Health
656 Perspectives, 116, A302-A305, 2008.

657 Wu, G. X., Li, Z. Q., Fu, C. B., Zhang, X. Y., Zhang, R. Y., Zhang, R. H., Zhou, T. J., Li, J.
658 P., Li, J. D., Zhou, D. G., Wu, L., Zhou, L. T., He, B., and Huang, R. H.: Advances in
659 studying interactions between aerosols and monsoon in China, Science China-Earth
660 Sciences, 59, 1-16, 10.1007/s11430-015-5198-z, 2016.

661 Wu, J., Li, G., Cao, J., Bei, N., Wang, Y., Feng, T., Huang, R., Liu, S., Zhang, Q., and Tie, X.:

662 Contributions of trans-boundary transport to summertime air quality in Beijing, China,
663 Atmospheric Chemistry and Physics, 17, 1-46, 2017.

664 Xu, J., Zhang, X. L., Xu, X. F., Zhao, X. J., Meng, W., and Pu, W. W.: Measurement of
665 surface ozone and its precursors in urban and rural sites in Beijing, in: Second
666 International Conference on Mining Engineering and Metallurgical Technology, edited
667 by: Zhu, R., Procedia Earth and Plantetary Science, Elsevier Science Bv, Amsterdam,
668 255-261, 2011.

669 Zhang, L., Liao, H., and Li, J. P.: Impacts of Asian summer monsoon on seasonal and
670 interannual variations of aerosols over eastern China, Journal of Geophysical
671 Research-Atmospheres, 115, 20, 10.1029/2009jd012299, 2010.

672 Zhang, Q., Streets, D. G., Carmichael, G. R., He, K. B., Huo, H., Kannari, A., Klimont, Z.,
673 Park, I. S., Reddy, S., Fu, J. S., Chen, D., Duan, L., Lei, Y., Wang, L. T., and Yao, Z. L.:
674 Asian emissions in 2006 for the NASA INTEX-B mission, Atmospheric Chemistry and
675 Physics, 9, 5131-5153, 2009.

676 Zhang, Q. Y., Tao, S. Y., and Chen, L. T.: The inter-annual variability of East Asian summer
677 monsoon indices and its association with the pattern of general circulation over East Asia
678 (in Chinese), Acta Meteorological Sinca, 61, 559-568, 2003.

679 Zhang, R., Khalizova, A. F., Wang, L., Hu, M., and Xu, W.: Nucleation and growth of
680 nanoparticles in the atmosphere, Chemical Reviews. 112, 1957–2011, 2012.

681 Zhang, R., Jing, J., Tao, J., Hsu, S. C., Wang, G., Cao, J., Lee, C. S. L., Zhu, L., Chen, Z.,
682 Zhao, Y., and Shen, Z.: Chemical characterization and source apportionment of $PM_{2.5}$ in
683 Beijing: seasonal perspective, Atmospheric Chemistry and Physics, 13, 7053-7074,
684 10.5194/acp-13-7053-2013, 2013.

685 Zhang, R. Y., Wang, G. H., Guo, S., Zarnora, M. L., Ying, Q., Lin, Y., Wang, W. G., Hu, M.,
686 and Wang, Y.: Formation of Urban Fine Particulate Matter, Chemical Reviews, 115,
687 3803-3855, 10.1021/acs.chemrev.5b00067, 2015.

688 Zhao, J., Levitt, N. P., Zhang, R. Y., and Chen, J. M.: Heterogeneous reactions of
689 methylglyoxal in acidic media: implications for secondary organic aerosol formation,
690 Environmental Science and Technology, 40, 7682–7687, 2006.

691 Zhao, C., Wang, Y. H., Yang, Q., Fu, R., Cunnold, D., and Choi, Y.: Impact of East Asian
692 summer monsoon on the air quality over China: View from space, Journal of Geophysical
693 Research-Atmospheres, 115, 12, 10.1029/2009jd012745, 2010.

694 Zhao, X. J., Zhao, P. S., Xu, J., Meng, W., Pu, W. W., Dong, F., He, D., and Shi, Q. F.:
695 Analysis of a winter regional haze event and its formation mechanism in the North China
696 Plain, Atmospheric Chemistry and Physics, 13, 5685-5696, 10.5194/acp-13-5685-2013,
697 2013.

698 Zhu, B., Akimoto, H., Wang, Z., Sudo, K., Tang, J., and Uno, I.: Why does surface ozone
699 peak in summertime at Waliguan?, Geophysical Research Letters, 31, 4,
700 10.1029/2004gl020609, 2004.

701 Zhu, J. L., Liao, H., and Li, J. P.: Increases in aerosol concentrations over eastern China due
702 to the decadal-scale weakening of the East Asian summer monsoon, Geophysical
703 Research Letters, 39, 6, 10.1029/2012gl051428, 2012.

704 Zhuang, X. L., Wang, Y. S., He, H., Liu, J. G., Wang, X. M., Zhu, T. Y., Ge, M. F., Zhou, J.,
705 Tang, G. Q., and Ma, J. Z.: Haze insights and mitigation in China: An overview, Journal
706 of Environmental Sciences, 26, 2-12, 10.1016/s1001-0742(13)60376-9, 2014.

707

708

709

710

711

712 Table 1 WRF-CHEM model configurations

713

Regions	Northern China
Simulation period	May 22 to 28, 2015
Domain size	350 × 350
Domain center	35°N, 114°E
Horizontal resolution	10km × 10km
Vertical resolution	35 vertical levels with a stretched vertical grid with spacing ranging from 30 m near the surface, to 500 m at 2.5 km and 1 km above 14 km
Microphysics scheme	WSM 6-class graupel scheme (Hong and Lim, 2006)
Boundary layer scheme	MYJ TKE scheme (Janjić, 2002)
Surface layer scheme	MYJ surface scheme (Janjić, 2002)
Cumulus scheme	Kain-Fritsch (new Eta) scheme (Kain, 2004)
Land-surface scheme	Unified Noah land-surface model (Chen and Dudhia, 2001)
Longwave radiation scheme	Goddard longwave scheme (Chou and Suarez, 2001)
Shortwave radiation scheme	Goddard shortwave scheme (Chou and Suarez, 1999)
Meteorological boundary and initial conditions	NCEP 1°×1° reanalysis data
Chemical initial and boundary conditions	MOZART 6-hour output (Horowitz et al., 2003)
Anthropogenic emission inventory	SAPRC-99 chemical mechanism emissions (Zhang et al., 2009)
Biogenic emission inventory	MEGAN model developed by Guenther et al. (2006)
Model spin-up time	28 hours

714

715

716

Table 2 Daily average $PM_{2.5}$ contributions (μg m^{-3}) of the NCP emissions in the NEC and NWC from 22 to 28 May 2015.

Date	Jilin	Liaoning	Shanxi	Shaanxi	Inner Mongolia
22	0.7±0.4	6.1±4.5	0.7±1.1	0.1±0.0	0.2±0.1
23	6.1±2.1	15.4±4.6	4.7±5.5	0.5±0.3	1.0±0.5
24	10.0±2.1	19.6±5.8	12.7±5.0	3.5±1.6	2.2±1.3
25	14.4±4.4	33.6±8.9	14.6±5.1	6.0±1.7	2.6±1.8
26	6.4±2.8	24.1±9.5	16.3±5.7	9.1±1.8	1.9±0.8
27	11.4±3.6	46.7±12.3	20.7±7.3	11.6±2.2	3.2±1.9
28	18.0±7.4	23.7±8.5	27.5±9.0	14.9±4.4	6.9±3.4
Average (μg m^{-3})	9.6±3.3	24.2±7.7	13.9±5.5	6.5±1.7	2.6±1.4
Average (%)	27.5±7.8	40.6±9.7	32.2±9.4	20.9±4.1	16.7±6.5

Table 3 Daily afternoon (12:00-18:00 BJT) average O_3 contributions (μg m^{-3}) of the NCP emissions in the NEC and NWC from 22 to 28 May 2015.

Date	Jilin	Liaoning	Shanxi	Shaanxi	Inner Mongolia
22	12.4±0.1	23.9±2.7	12.7±0.0	7.7±0.0	2.8±0.0
23	25.8±2.5	38.9±6.2	21.5±1.1	13.1±0.3	5.1±0.2
24	35.0±3.6	47.5±8.1	31.3±3.9	21.2±1.9	8.5±0.5
25	45.7±8.4	69.5±15.5	39.7±6.4	21.5±2.5	9.9±0.6
26	16.6±1.6	41.0±5.9	36.4±4.6	21.7±2.4	10.8±0.7
27	23.9±5.0	69.3±16.4	51.7±7.8	33.5±4.5	9.6±1.0
28	41.7±5.5	35.1±6.5	52.3±9.0	26.5±4.7	12.2±1.8
Average (μg m^{-3})	28.7±3.8	46.5±8.8	35.1±4.7	20.7±2.3	8.4±0.7
Average (%)	19.5±2.9	27.4±5.9	21.2±3.2	15.8±2.0	8.0±0.7

Figure Captions

Figure 1 WRF-CHEM simulation domain with topography. The blue circles represent centers of cities with ambient monitoring sites and the red circle denotes the NCNST site. The size of the blue circle represents the number of ambient monitoring sites of cities.

Figure 2 (a) Geopotential heights and (b) the mean sea level pressures with wind vectors during the summer monsoon season in 2015.

Figure 3 Relationships of observed $PM_{2.5}$ and O_3 concentrations in NCP with those in the NEC during May to September from 2013 to 2016.

Figure 4 Same as Figure 3, but for the NWC.

Figure 5 Comparison of measured (black dots) and predicted (blue line) diurnal profiles of near-surface hourly (a) $PM_{2.5}$, (b) O_3, and (c) NO_2 averaged over all ambient monitoring stations in Northern China from 22 to 28 May 2015.

Figure 6 Comparison of measured (black dots) and simulated (black line) diurnal profiles of submicron aerosol species of (a) POA, (b) SOA, (c) sulfate, (d) nitrate, and (e) ammonium at NCNST site in Beijing from 22 to 28 May 2015.

Figure 7 Pattern comparison of simulated vs. observed near-surface $PM_{2.5}$ at 08:00 BJT during from 23 to 28 May 2015. Colored circles: $PM_{2.5}$ observations; color contour: $PM_{2.5}$ simulations; black arrows: simulated surface winds.

Figure 8 Same as Figure 7, but for the near-surface O_3 at 14:00 BJT.

Figure 9 Contributions of NCP emissions to the daily mean near-surface $PM_{2.5}$ concentration in the NEC and NWC from 23 to 28 May 2015.

Figure 10 Average percentage contribution of NCP emissions to $PM_{2.5}$ concentrations in the NEC and NWC from 22 to 28 May 2015.

Figure 11 Same as Figure 9, but for the afternoon (12-18:00 BJT) O_3 concentration.

Figure 12 Same as Figure 10, but for the afternoon (12-18:00 BJT) O_3 concentration.

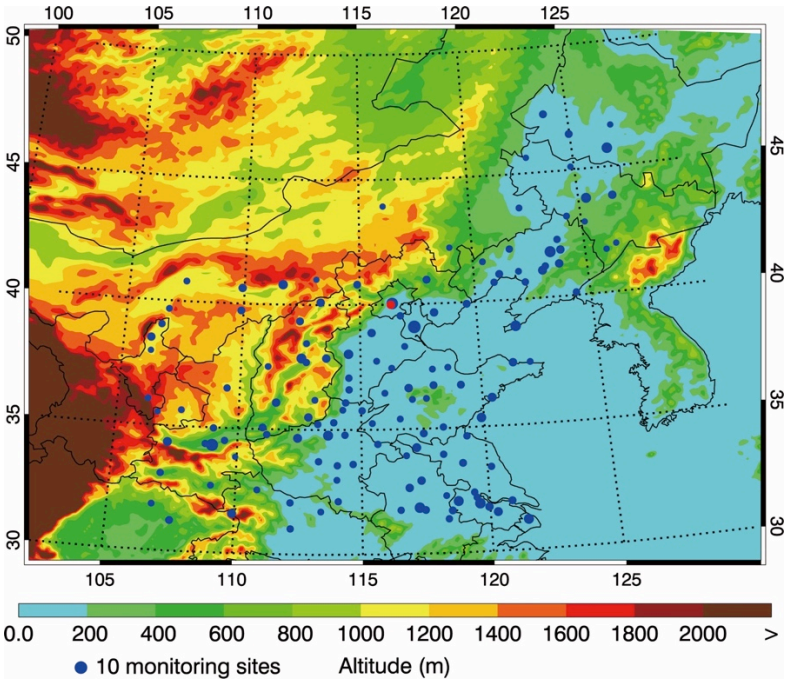

Figure 1 WRF-CHEM simulation domain with topography. The blue circles represent centers of cities with ambient monitoring sites and the red circle denotes the NCNST site. The size of the blue circle represents the number of ambient monitoring sites of cities.

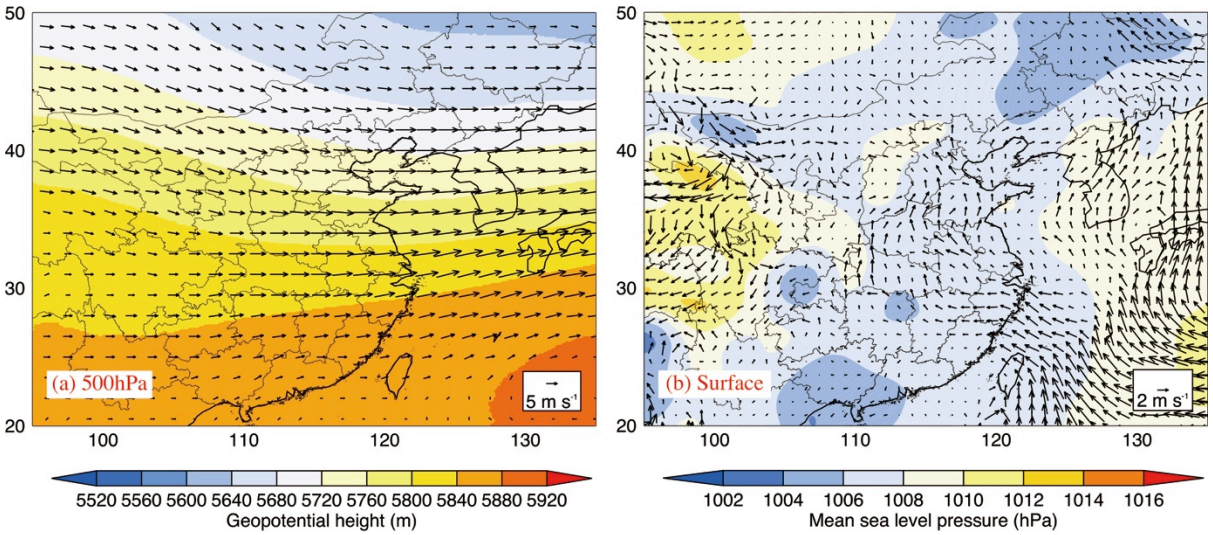

773
774
775 Figure 2 (a) Geopotential heights and (b) the mean sea level pressures with wind vectors
776 during the summer monsoon season in 2015.

777
778
779
780
781

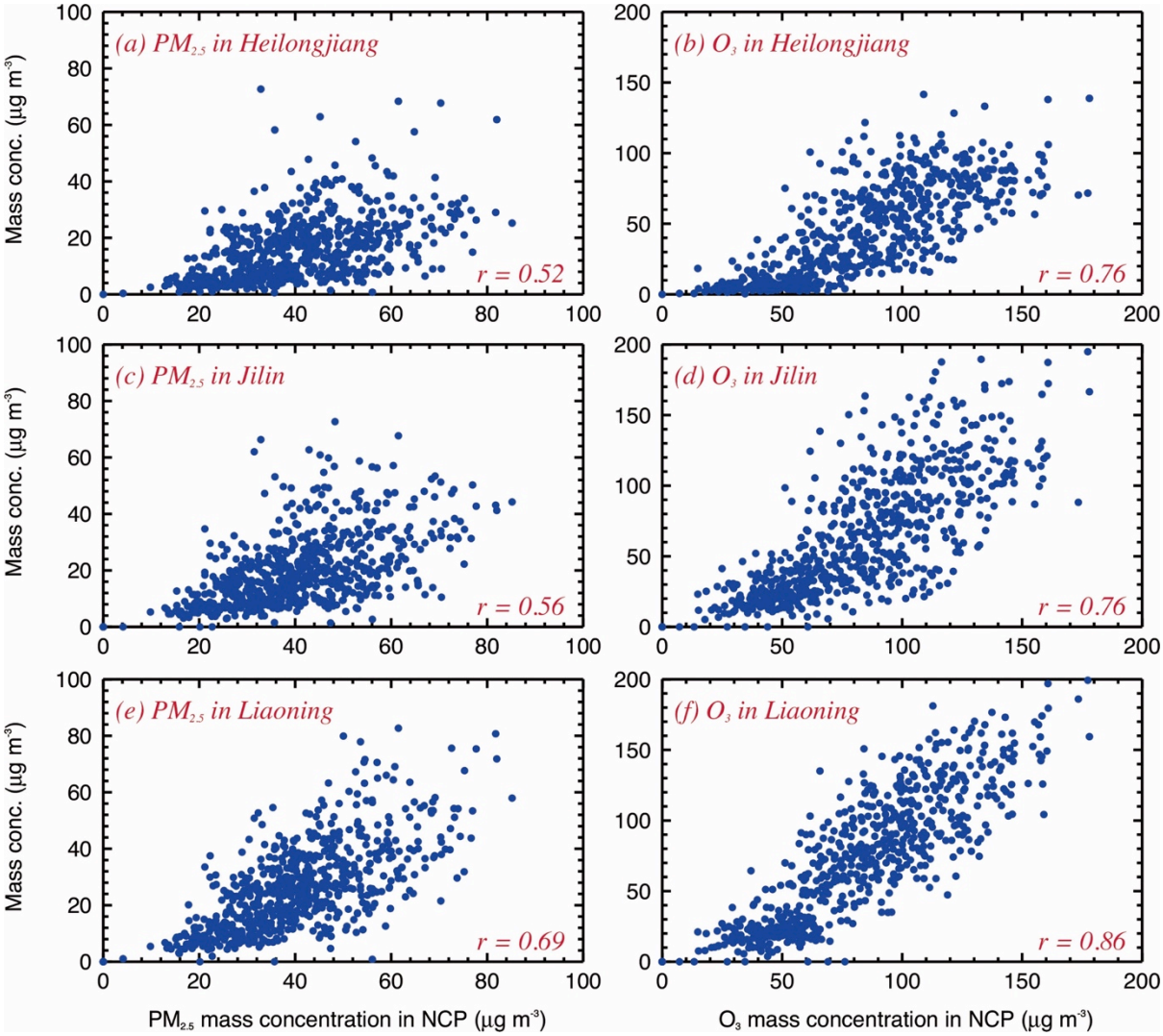

Figure 3 Relationships of observed $PM_{2.5}$ and O_3 concentrations in NCP with those in the NEC during May to September from 2013 to 2016.

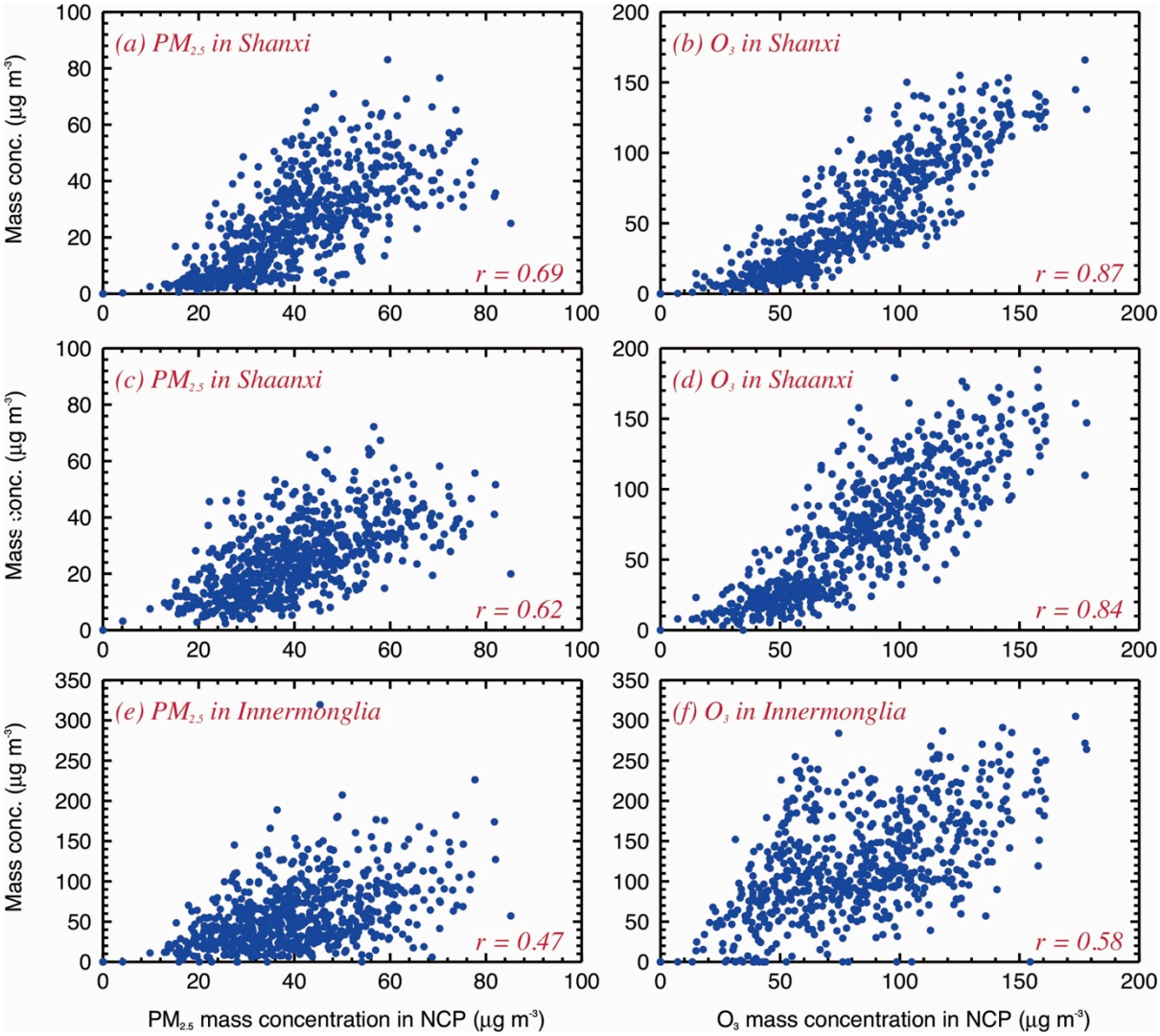

Figure 4 Same as Figure 3, but for the NWC.

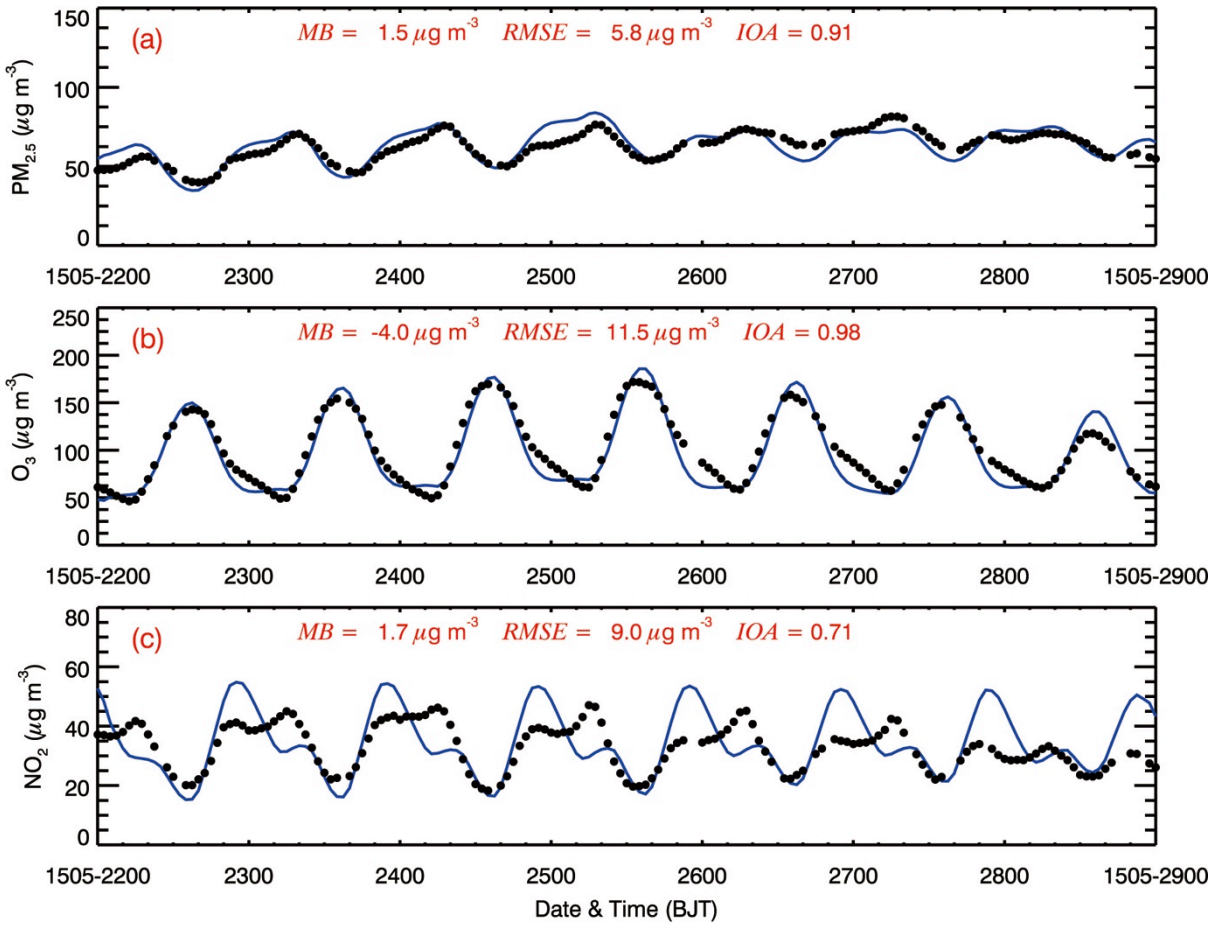

Figure 5 Comparison of measured (black dots) and predicted (blue line) diurnal profiles of near-surface hourly (a) $PM_{2.5}$, (b) O_3, and (c) NO_2 averaged over all ambient monitoring stations in Northern China from 22 to 28 May 2015

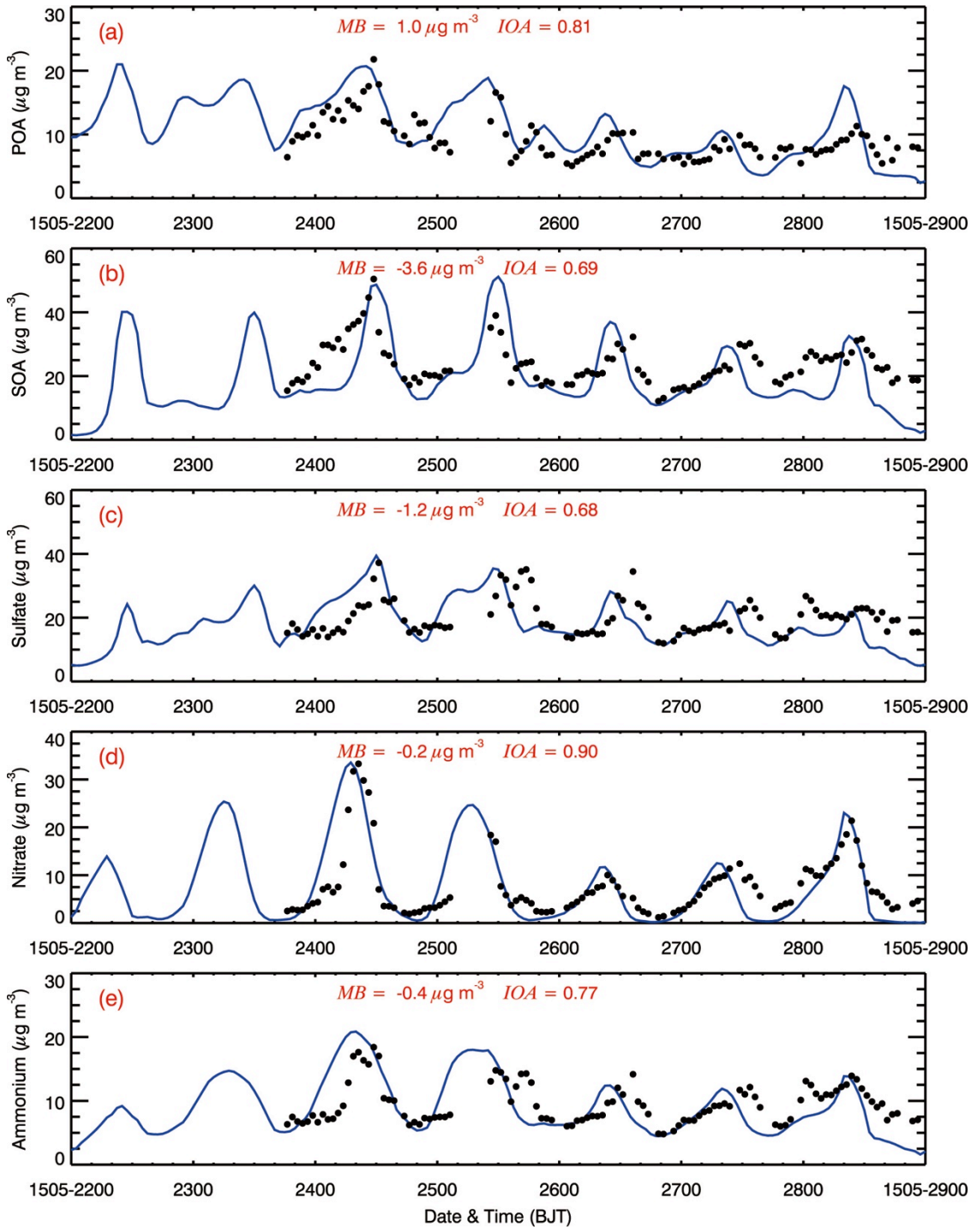

Figure 6 Comparison of measured (black dots) and simulated (black line) diurnal profiles of submicron aerosol species of (a) POA, (b) SOA, (c) sulfate, (d) nitrate, and (e) ammonium at NCNST site in Beijing from 22 to 28 May 2015.

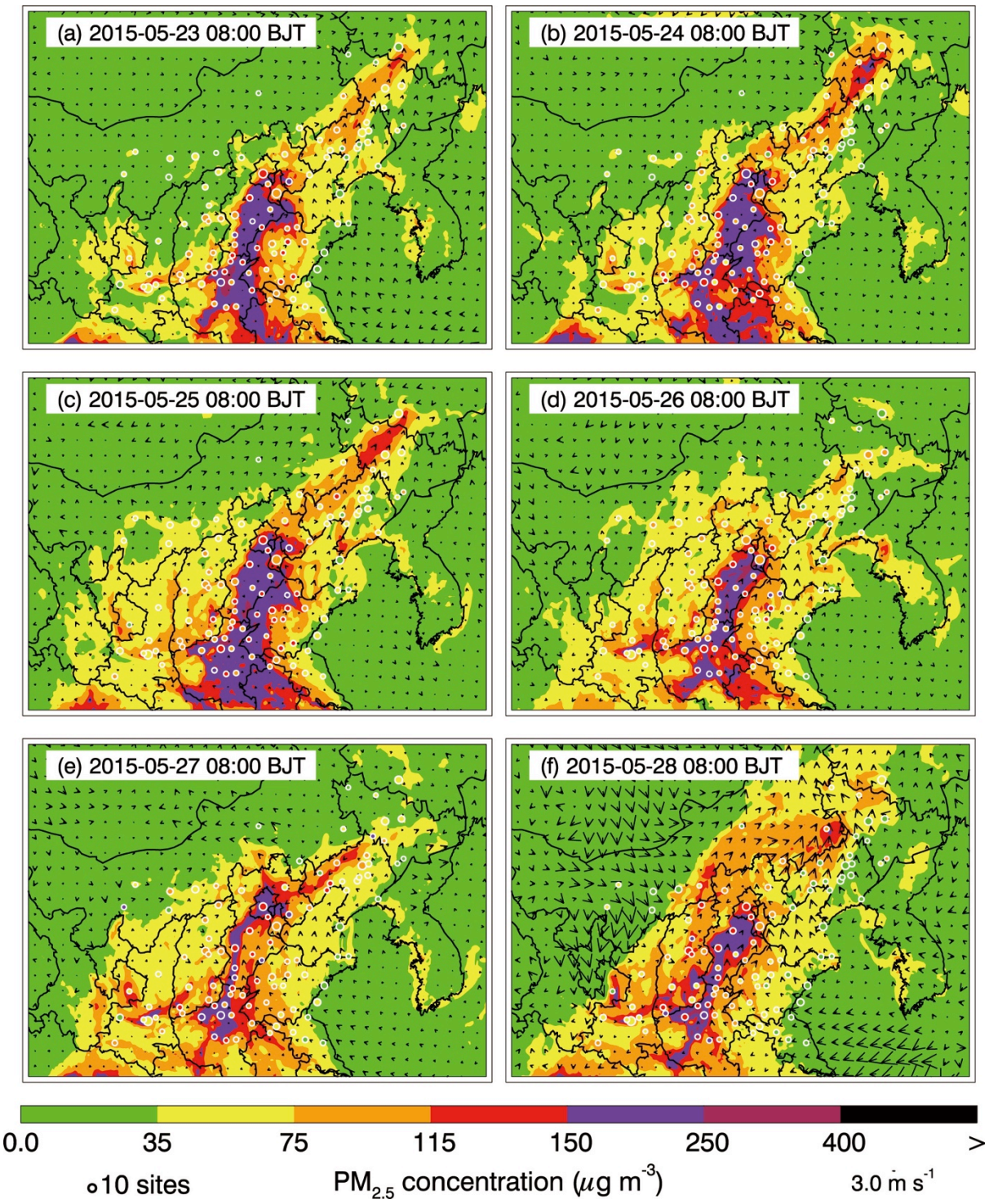

Figure 7 Pattern comparison of simulated vs. observed near-surface $PM_{2.5}$ at 08:00 BJT during from 23 to 28 May 2015. Colored circles: $PM_{2.5}$ observations; color contour: $PM_{2.5}$ simulations; black arrows: simulated surface winds.

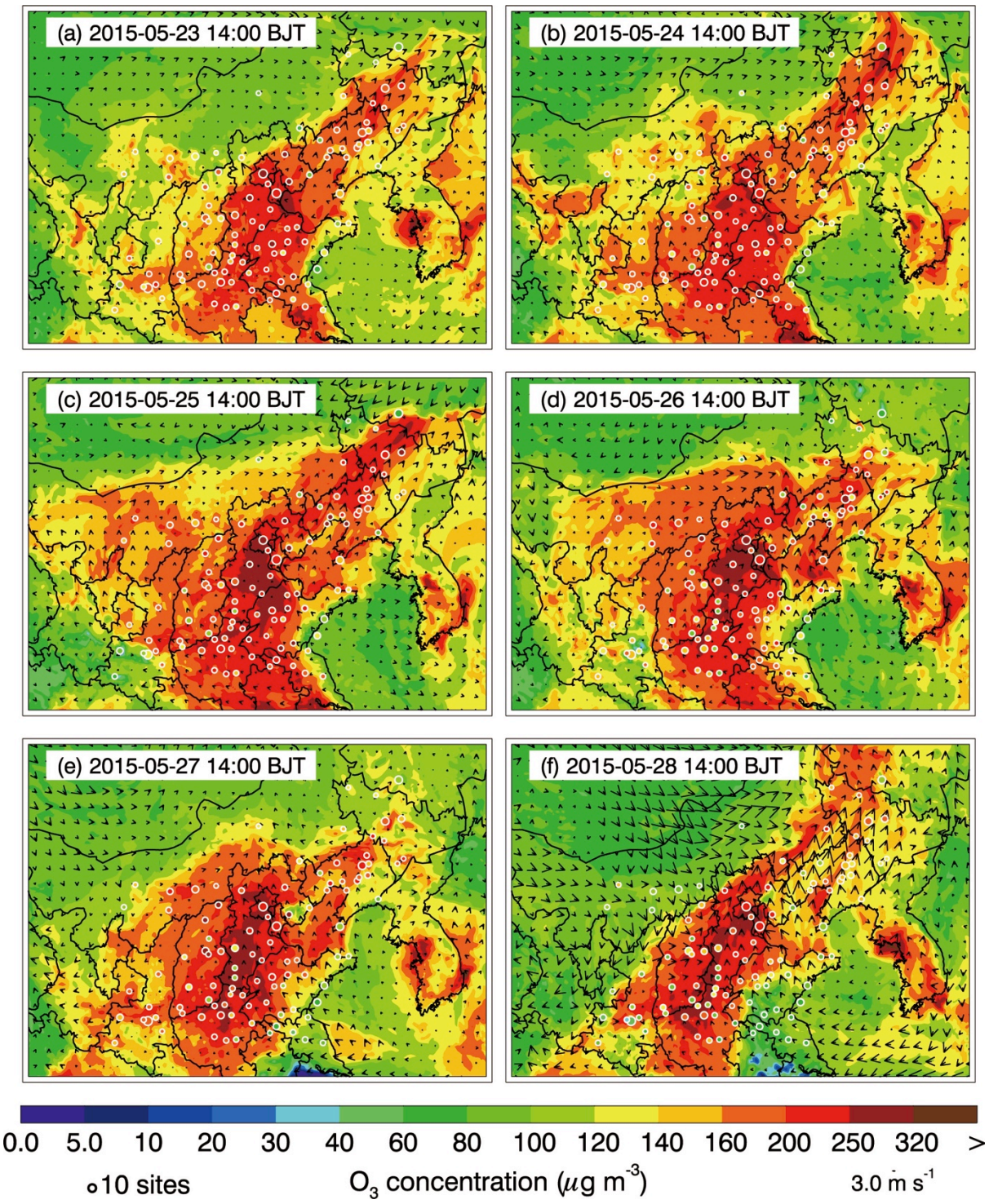

Figure 8 Same as Figure 7, but for the near-surface O_3 at 14:00 BJT.

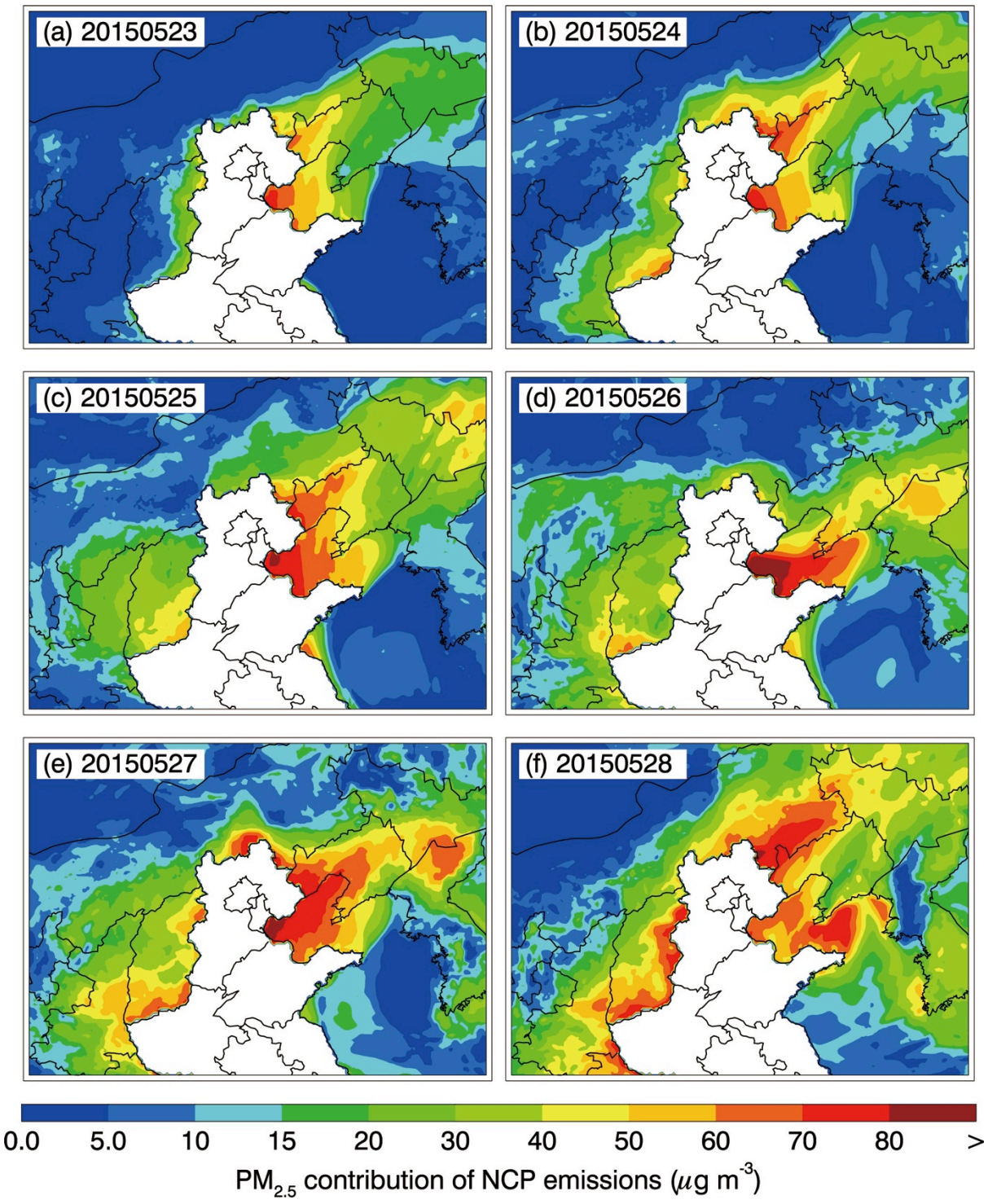

Figure 9 Contributions of NCP emissions to the daily mean near-surface $PM_{2.5}$ concentration in the NEC and NWC from 23 to 28 May 2015.

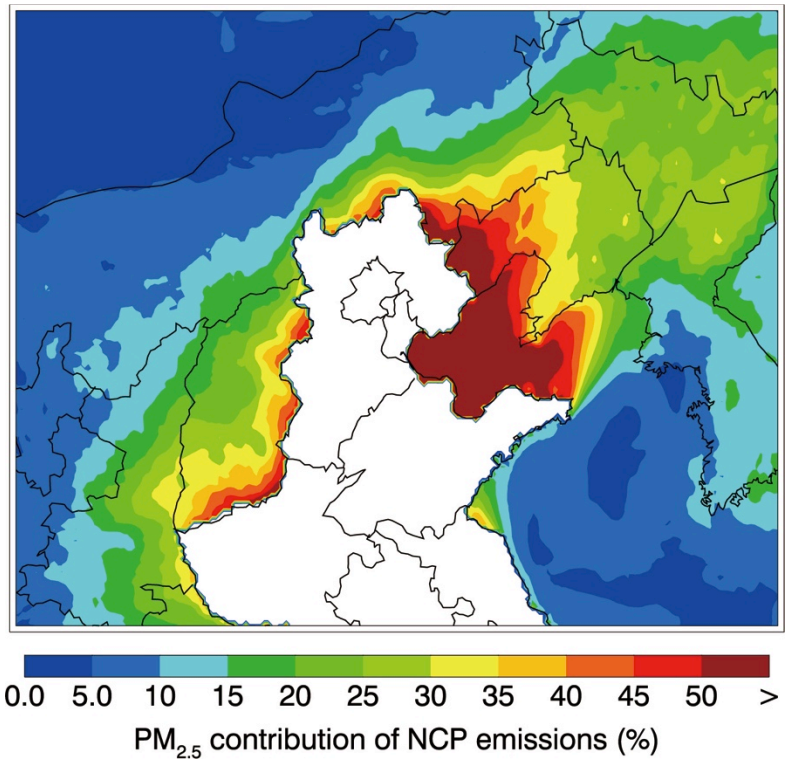

Figure 10 Average percentage contribution of NCP emissions to $PM_{2.5}$ concentrations in the NEC and NWC fron 22 to 28 May 2015.

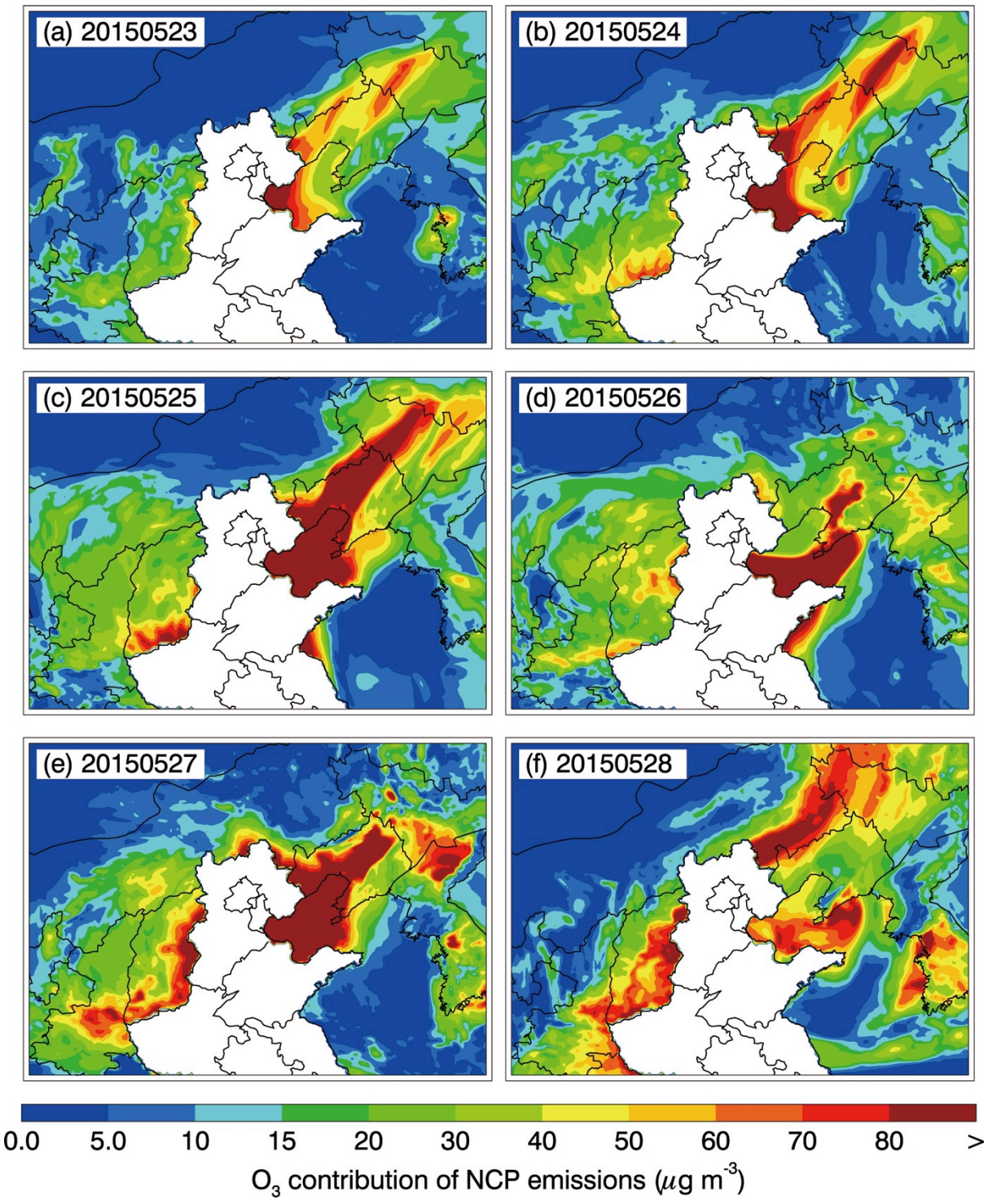

Figure 11 Same as Figure 9, but for the afternoon (12-18:00 BJT) O_3 concentration.

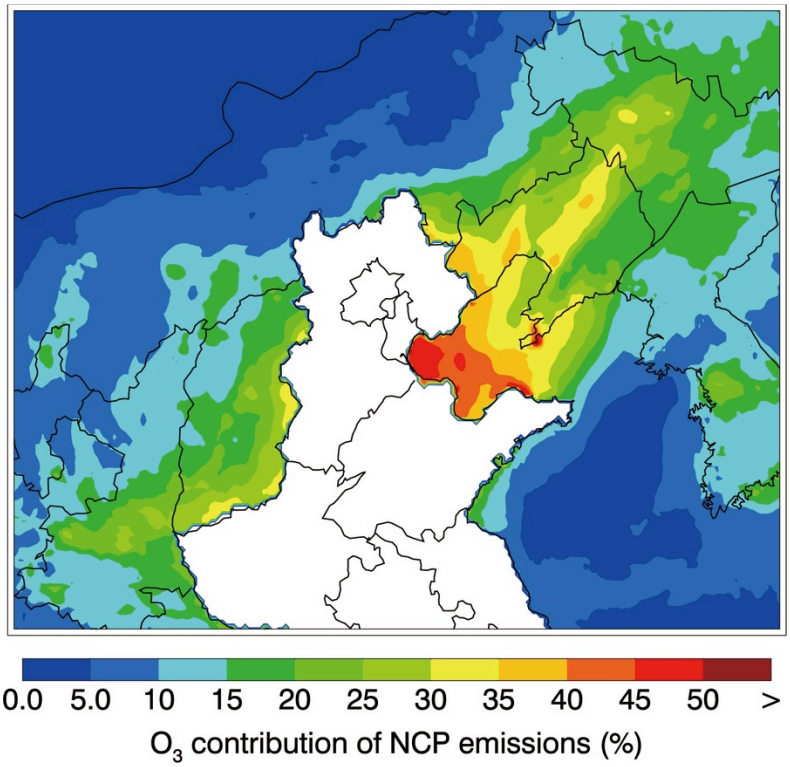

Figure 12 Same as Figure 10, but for the afternoon (12-18:00 BJT) O_3 concentration.